



Short communication

# A finite shell element for heart mitral valve leaflet mechanics, with large deformations and 3D constitutive material model

Eli J. Weinberg<sup>a,b</sup>, Mohammad R. Kaazempur Mofrad<sup>c,\*</sup>

<sup>a</sup>*Massachusetts Institute of Technology, Department of Mechanical Engineering, Cambridge, MA, USA*

<sup>b</sup>*Draper Laboratory, Cambridge, MA, USA*

<sup>c</sup>*Department of Bioengineering, University of California Berkeley, 483 Evans Hall #1762, Berkeley, CA 94720, USA*

Accepted 6 January 2006

---

## Abstract

This paper presents a shell finite element formulation appropriate for simulating the heart valve leaflet mechanics, including three-dimensional (3D) stress and strain effects. A 4-node mixed-interpolation shell is formulated in convected coordinates. This shell model is made capable of handling arbitrary 3D material models by use of an algorithm that satisfies the shell stress assumption at every element integration point. A method for tracking the fiber direction is incorporated. The resulting shell element operates under the same conditions as a standard 4-node shell element with 5 degrees of freedom per node, but extends the modeling capabilities to handle large-deformation and anisotropic behavior.

© 2006 Elsevier Ltd. All rights reserved.

*Keywords:* Mitral valve; Shell element; Incompressible; Transversely isotropic; Large strain

---

## 1. Introduction

A number of finite element simulations of dynamic heart valve behavior have been published (see review in Weinberg and Kaazempur-Mofrad, 2005a). Material and element formulations used in these simulations include a membrane element with structural material (Einstein et al., 2004), nonlinear elastic shell (Votta et al., 2002), linear elastic solid (Hart et al., 2003), and linear elastic shell (Kunzelman et al., 1993). The authors are not aware of any work that includes the 3D stress state and accounts for large-deformation behavior, particularly through-thickness strain. The aim of this paper is to formulate an element that accurately describes the large-deformation 3D stress-strain behavior of mitral valve leaflet tissue and readily fits within the setting of existing finite element software.

The material comprising the mitral valve leaflets is considered to be hyperelastic, incompressible, and transversely isotropic (May-Newman and Yin, 1998). One way to implement this description of such a material in the finite-element setting is to use 3D elements with a mixed pressure-displacement formulation (Weinberg and Kaazempur-Mofrad, 2005b). However, accurate results of the bending behavior require a high-order element and fine meshing that exert formidable computational expense. To handle this simulation more efficiently, we propose here a shell element formulation that includes the 3D constitutive material model.

In large-deformation shell calculations, the through-thickness strain contributes significantly to the stress response and stiffness tensor. This strain cannot be calculated using the standard interpolations used for other strains, but a variety of ways to calculate the through-thickness strain have been described. 3D shell elements are attractive, in that they generally do not require manipulation of the material model to fit shell

---

\*Corresponding author. Tel.: +1 510 643 8165;  
fax: +1 510 642 5835.

*E-mail address:* mofrad@berkeley.edu (M.R. Kaazempur Mofrad).

stress assumptions (Chapelle et al., 2004; Sze et al., 2004). Methods to incorporate a 3D material model into a conventional shell by use of an extensible normal vector have received much attention (Betsch et al., 1996; Simo et al., 1990; Basar et al., 2003). A simpler method to achieve the same has been proposed by Klinkel and Govindjee (2002). Both conventional shell methods are expected to be cheaper than the 3D shell in our case. The 3D shell model will require significantly more nodes than a conventional shell, particularly requiring multiple nodes through the thickness to represent bending behavior. Additionally, for an incompressible material like that of mitral leaflet tissue, the 3D shell model may require the added complexity of a mixed pressure-displacement formulation (Sussman and Bathe, 1987) that the conventional shell will not. We have chosen to use the latter shell method on the basis that it is more computationally efficient than methods involving the extensible normal (Klinkel and Govindjee, 2002) and that, unlike methods with an extensible normal, it does not require additional degrees of freedom (DOF) compared to the standard 4-node shell element with 5-DOF per node commonly found in finite element software.

A 4-node quadrilateral with mixed interpolation of the transverse strains is currently accepted as the most cost-effective shell (Bathe, 1996). This shell is implemented (Dvorkin, 1984) and the local plane stress algorithm of Klinkel and Govindjee (2002) is used to incorporate the 3D material models. We define a fiber-aligned coordinate system, which allows simple interfacing between anisotropic material calculations and plane stress algorithm. As a demonstration, an existing constitutive material equation leaflet tissue (May-Newman and Yin, 1998) is applied and numerical results are shown to match in-plane analytical results. A test case is shown demonstrating function of the element and influence of fiber direction.

## 2. Methods

In this section, we first outline the equations used in the standard 4-node shell element with 5-DOF per node, known as MITC4 element. Following that, we describe methods for incorporating the fiber-aligned coordinate system and through-thickness strain calculation into this shell element.

### 2.1. Continuum mechanics and shell definitions

The underlying equations for the MITC4 shell element are standard large-deformation solid mechanics and shell equations. The deformation gradient is

denoted as

$$\mathbf{F} = \frac{\partial \mathbf{x}}{\partial \mathbf{X}}, \quad (1)$$

where  $\mathbf{X}$  is the original (undeformed) configuration and  $\mathbf{x}$  is the deformed configuration.

The shell calculations are performed in the Green–Lagrange strain tensor,

$$\boldsymbol{\varepsilon} = \frac{1}{2}(\mathbf{F}^T \cdot \mathbf{F} - \mathbf{I}), \quad (2)$$

where  $\mathbf{I}$  is the identity tensor.

The right Cauchy–Green deformation tensor is

$$\mathbf{C} = \mathbf{F}^T \cdot \mathbf{F} = 2\boldsymbol{\varepsilon} + \mathbf{I}, \quad (3)$$

the strain invariants in terms of  $\mathbf{C}$  are

$$\begin{aligned} I_1 &= \text{tr } \mathbf{C}, \\ I_2 &= \frac{1}{2}((\text{tr } \mathbf{C})^2 - \text{tr } \mathbf{C}^2), \\ I_3 &= \det \mathbf{C}, \end{aligned} \quad (4)$$

and the Jacobian is  $J = \sqrt{I_3}$ . Transverse isotropy is incorporated into the model by introducing a vector that defines the preferred fiber direction of the material. Denoting the vector as  $\mathbf{N}$ , the stretch in the fiber direction is

$$\alpha = \sqrt{\mathbf{N} \cdot \mathbf{C} \cdot \mathbf{N}}, \quad (5)$$

and two pseudo-invariants can be defined in terms of the right Cauchy–Green strain (Spencer, 1972):

$$\begin{aligned} I_4 &= \mathbf{N} \cdot \mathbf{C} \cdot \mathbf{N} = \alpha^2, \\ I_5 &= \mathbf{N} \cdot \mathbf{C}^2 \cdot \mathbf{N}. \end{aligned} \quad (6)$$

The stress state is calculated from the deformation state based on a strain energy function,  $W$ ,

$$\mathbf{S} = \frac{\partial W}{\partial \boldsymbol{\varepsilon}} = 2 \frac{\partial W}{\partial \mathbf{C}}, \quad (7)$$

where  $\mathbf{S}$  is the 2nd Piola–Kirchhoff stress tensor. The material constitutive tensor is

$$\mathbf{C} = \frac{\partial^2 W}{\partial \boldsymbol{\varepsilon}^2} = 4 \frac{\partial^2 W}{\partial \mathbf{C}^2}. \quad (8)$$

The three invariants described in Eq. (4) are recognized to describe isotropic hyperelasticity. Spencer (1972) has shown that the full set of five invariants, defined in Eqs. (4) and (6) can be used to describe the strain-energy function of transversely isotropic hyperelasticity.

The 4-node shell element with 5-DOF per node, known as the MITC4, is described in convected coordinates and uses mixed interpolation of the transverse strains to avoid locking (Dvorkin, 1984; Dvorkin and Bathe, 1984). Here we outline the basis of this formulation. In the global Cartesian coordinate system ( $e_1, e_2, e_3$ ), the coordinates ( $x_1, x_2, x_3$ ) of a particle having natural shell coordinate ( $r_1, r_2, r_3$ ) is

$${}^t x_i = h_k {}^t x_i^k + \frac{r_3}{2} {}^t a_k h_k {}^t V_{mi}^k, \quad (9)$$

where  $x^k$  is the global position of node  $k$ ,  $V_n$  is the director vector at node  $k$ ,  $h_k(r_1, r_2)$  is the interpolation function corresponding to node  $k$ ,  ${}^t a_k$  is the thickness at node  $k$  measured in the direction of  $V_n$ . We allow the thickness  ${}^t a_k$  to vary in time (Dvorkin et al., 1995) both due to changes in the physical shell thickness and due to the rotation of  $V_n$ . Throughout, the left superscript  $t$  refers to the time and the right subscript  $i$  refers to the component in the  $x_i$  direction. Local orthogonal vectors are defined:

$$\begin{aligned} {}^0 \mathbf{V}_1^k &= \frac{\mathbf{e}_2 \times {}^0 \mathbf{V}_n^k}{|\mathbf{e}_2 \times {}^0 \mathbf{V}_n^k|}, \\ {}^0 \mathbf{V}_2^k &= {}^0 \mathbf{V}_n^k \times {}^0 \mathbf{V}_1^k, \end{aligned} \quad (10)$$

and the rotation of these vectors in time is achieved by rotation matrix (Argyris, 1982).

The displacement  ${}^t u_i$  and incremental displacement  $u_i$  are

$$\begin{aligned} {}^t u_i &= h_k {}^t u_i^k + \frac{r_3}{2} {}^t a_k h_k ({}^t V_{ni}^k - {}^0 V_{ni}^k), \\ u_i &= h_k u_i^k + \frac{r_3}{2} {}^t a_k h_k (-{}^t V_{2i}^k \alpha_k + {}^t V_{1i}^k \beta), \end{aligned} \quad (11)$$

where  $\alpha$  and  $\beta$  are the rotational DOF. Covariant base vectors are given by

$${}^t \mathbf{g}_i = \frac{\partial {}^t \mathbf{x}}{\partial r_i} \quad (12)$$

and the contravariant base vectors  ${}^t \mathbf{g}^i$  are calculated to satisfy  ${}^t \mathbf{g}_i \cdot {}^t \mathbf{g}^j = \delta_{ij}$ . The Green–Lagrange strains are calculated in the covariant system,

$${}^t \tilde{\epsilon}_{ij} = \frac{1}{2} ({}^t \mathbf{g}_i \cdot {}^t \mathbf{g}_j - {}^0 \mathbf{g}_i \cdot {}^0 \mathbf{g}_j), \quad (13)$$

where the tilde overbar denotes values measured in the covariant system.

The Green–Lagrange strains are transformed from the covariant system to the Cartesian local,

$$\hat{\epsilon}_{ij} = ({}^0 \mathbf{g}^i \cdot {}^t \hat{\mathbf{e}}_m) ({}^0 \mathbf{g}^j \cdot {}^t \hat{\mathbf{e}}_n) {}^t \tilde{\epsilon}_{mn}. \quad (14)$$

The constitutive material tensor in the local Cartesian coordinate system is denoted  $\hat{\mathbf{C}}$ , which contains the shell assumption of zero stress in the through-thickness direction. This tensor may be calculated as in Eq. (8) using the Green–Lagrange strain in Cartesian coordinates (Eq. 14). The constitutive tensor is made to relate the incremental covariant strains to the incremental contravariant stresses by the transformation:

$$\tilde{\mathbf{C}}^{ijkl} = ({}^t \mathbf{g}^i \cdot \hat{\mathbf{e}}_m) ({}^t \mathbf{g}^j \cdot \hat{\mathbf{e}}_n) ({}^t \mathbf{g}^k \cdot \hat{\mathbf{e}}_o) ({}^t \mathbf{g}^l \cdot \hat{\mathbf{e}}_p) \hat{\mathbf{C}}^{mnop}. \quad (15)$$

The stresses are calculated in the local Cartesian coordinates as in Eq. (7), then transformed to the covariant coordinates,

$$\tilde{\mathbf{S}}^{ij} = ({}^t \hat{\mathbf{e}}_m \cdot {}^t \mathbf{g}^i) ({}^t \hat{\mathbf{e}}_n \cdot {}^t \mathbf{g}^j) \hat{\mathbf{S}}_{mn}. \quad (16)$$

All strain components are computed in the standard manner (Bathe, 1996), except for the transverse shear

strains which are found using separate interpolations to avoid locking:

$$\begin{aligned} \tilde{\epsilon}_{13}(r_1, r_2, r_3) &= \frac{1}{2} (1 + r_2) \tilde{\epsilon}_{13} \Big|_A \\ &\quad + \tilde{\epsilon}_{13}(r_1, r_2, r_3) = \frac{1}{2} (1 - r_2) \tilde{\epsilon}_{13} \Big|_C, \\ \tilde{\epsilon}_{23}(r_1, r_2, r_3) &= \frac{1}{2} (1 + r_1) \tilde{\epsilon}_{23} \Big|_D \\ &\quad + \tilde{\epsilon}_{13}(r_1, r_2, r_3) = \frac{1}{2} (1 + r_1) \tilde{\epsilon}_{23} \Big|_B, \end{aligned} \quad (17)$$

where  $A$  is the location ( $r_1 = 0, r_2 = 1, r_3 = 0$ ),  $B$  is ( $r_1 = -1, r_2 = 0, r_3 = 0$ ),  $C$  is ( $r_1 = 0, r_2 = -1, r_3 = 0$ ), and  $D$  is ( $r_1 = 1, r_2 = 0, r_3 = 0$ ).

In a total Lagrangian formulation with convected coordinates, the linearized equation of motion is

$$\begin{aligned} \int_{0V} {}^0 \tilde{\mathbf{C}}^{ijkl} {}^0 \tilde{\epsilon}_{kl} \delta_0 \tilde{\epsilon}_{ij}^0 dV + \int_{0V} {}^t {}_0 \tilde{\mathbf{S}}^{ij} \delta_0 \tilde{\eta}_{ij}^0 dV \\ = {}^{t+\Delta t} \mathfrak{R} - \int_{0V} {}^t {}_0 \tilde{\mathbf{S}}^{ij} \delta_0 \tilde{\epsilon}_{ij}^0 dV, \end{aligned} \quad (18)$$

where  $\tilde{\epsilon}_{ij}$  and  $\tilde{\eta}_{ij}$  are the linear and nonlinear parts of the Green–Lagrange strain components  $\tilde{\epsilon}_{ij}$  (Dvorkin and Bathe, 1984). All terms are calculated using the above definitions.

## 2.2. Fiber-aligned coordinate system

We introduce a particular Cartesian system for the current application. In heart valve leaflet tissue, the fiber direction lies in the element midplane (May-Newman and Yin, 1998). First the initial fiber direction  ${}^0 \mathbf{N}$  is defined in global coordinates and transformed in time, to give  ${}^t \mathbf{N}$ , by standard vector transform (Bathe, 1996). In heart valve leaflet tissue, the fiber direction lies in the plane of the leaflet (May-Newman and Yin, 1998), therefore we assume that the fiber direction lies parallel to the element mid-plane. We define a local fiber-aligned Cartesian coordinate system  $\hat{\mathbf{e}}$  by

$${}^t \hat{\mathbf{e}}_1 = \frac{{}^t \mathbf{N}}{|{}^t \mathbf{N}|}, {}^t \hat{\mathbf{e}}_3 = \frac{{}^t \mathbf{g}_1 \times {}^t \mathbf{g}_2}{|{}^t \mathbf{g}_1 \times {}^t \mathbf{g}_2|}, {}^t \hat{\mathbf{e}}_2 = {}^t \hat{\mathbf{e}}_3 \times {}^t \hat{\mathbf{e}}_1, \quad (19)$$

where the hat overbar denotes quantities measured in this system. The first direction of this system is parallel to the fiber direction, and the third direction is parallel to the through-thickness direction. This coordinate system is very convenient to use in the current application, as it is the only Cartesian system needed for both the material-based calculations and the following shell stress calculations. The material stress and tangent tensor calculations (Eqs. (7) and (8)) are performed in the  $\hat{\mathbf{e}}$  coordinate system with the fiber direction simply  ${}^t \hat{\mathbf{N}} = [1 \ 0 \ 0]$  at all times, and the plane-stress algorithm described below is performed with the through-thickness direction simply parallel to  ${}^t \hat{\mathbf{e}}_3$ .

### 2.3. Local plane-stress algorithm for calculation of thickness, stresses and constitutive tensor

In the MITC shell formulation, the stresses and material stiffness tensor needed to compute the finite element matrices must reflect the shell stress assumption of zero through-thickness stress. Klinkel and Govindjee (2002) provide a simple, rigorous method for incorporating an arbitrary 3D material model into a shell element. They refer to this method as the local plane stress algorithm. The essence of this method is that the standard 5-DOF per node shell does not provide a way to interpolate the through-thickness strain. Instead, this method calculates the through-thickness strain at each integration point, so that the shell stress assumption is satisfied, and then calculates the stresses and material stiffness tensor needed for the finite element matrices. Additionally, the thickness  $t_k$  in the direction of  $V_n$  is updated by running the local plane stress algorithm at each node.

Here we outline the necessary steps of the algorithm. For a full discussion of this method, see Klinkel and Govindjee, 2002. In this method, the stress vector, strain vector, and stiffness tensor are partitioned:

$$\begin{bmatrix} \partial \hat{S}_m \\ \partial \hat{S}_z \end{bmatrix} = \begin{bmatrix} \hat{C}_{mm} \hat{C}_{mz} \\ \hat{C}_{zm} \hat{C}_{zz} \end{bmatrix} \begin{bmatrix} \partial \hat{\epsilon}_m \\ \partial \hat{\epsilon}_z \end{bmatrix}, \quad (20)$$

where, for the shell, we have the definitions

$$\hat{S}_m = [\hat{S}_{11} \hat{S}_{12} \hat{S}_{13} \hat{S}_{22} \hat{S}_{23}]^T, \quad \hat{S}_z = \hat{S}_{33}. \quad (21)$$

The stress, strain, and stiffness components here are those in the fiber-aligned system  $\hat{e}$  defined by Eq. (19). The following are the steps of the plane stress algorithm incorporated into the shell model. At each time step, this algorithm is run at each integration point to get the stress  $\hat{S}$  and stiffness  $\hat{C}$ , and is run at each node to update the thickness  $t_k$ .

1. The Green–Lagrange strains  $\hat{\epsilon}$ , not including the through-thickness strain, are calculated in the local Cartesian system.
2. An initial guess is made for the through-thickness strain  $\hat{\epsilon}_{33}$ . We use the value of  $\hat{\epsilon}_{33}$  from the previous converged iteration for this guess.
3. The second Piola–Kirchhoff stresses  $\hat{S}$  and material stiffness tensor  $\hat{C}$  are calculated by applying Eqs. (7) and (8), respectively to the strain energy function (Eq. (10)), with the fiber direction  $\hat{N} = [1 \ 0 \ 0]$ .
4. If  $\|\hat{S}_z\|$  is larger than a chosen tolerance, the through-thickness strain is updated by

$$\hat{\epsilon}_z^{i+1} = \hat{\epsilon}_z^i - \frac{\hat{S}_z^i}{\hat{C}_{zz}^i}, \quad (22)$$

and the method is returned to step 3. If the  $\|\hat{S}_z\|$  is smaller than a chosen tolerance, the algorithm

continues to step 4. The converged value for  $\hat{\epsilon}_z$  is the strain in the direction perpendicular to the shell midsurface, from which the change in thickness is directly found. At each node, the thickness for the next timestep  $t^{+\Delta t} a_k$  is found by projecting the physical thickness on the director vector  $V_n$ .

5. With  $\hat{S}_z = 0$ , the stiffness matrix can be condensed using

$$\hat{C}_{\text{condensed}} = \left[ \hat{C}_{mm} - \frac{1}{\hat{C}_{zz}} \hat{C}_{mz} \hat{C}_{zm} \right]. \quad (23)$$

6. A row and column of zeros are inserted into  $\hat{C}_{\text{condensed}}$  to represent the through-thickness direction, yielding the stiffness matrix with shell assumption  $\hat{C}$  in the local Cartesian system. At this step, the stresses  $\hat{S}$  are the stresses in the local fiber-aligned Cartesian system, with the through-thickness stress equal to zero within the chosen tolerance.

The stiffness tensor is then transformed to the natural shell coordinate system; the stresses are transformed to the covariant system (Eqs. (15) and (16)). Thus the stiffness tensor and stresses from a 3D constitutive model are incorporated into our shell.

### 2.4. Constitutive material model

To demonstrate this shell we use a strain-energy function that has previously been determined for mitral valve leaflet tissue through biaxial testing (May-Newman and Yin, 1998),

$$W(I_1, I_4) = c_0 \{ \exp[c_1(I_1 - 3)^2 + c_2(I_4^{1/2} - 1)^4] - 1 \}, \quad (24)$$

with one set of constants for the anterior leaflet and one set for the posterior (Table 1).

As in our previous work (Weinberg and Kaazempur-Mofrad, 2005b), a neo-Hookean term is added to avoid the zero matrix at low strains and a volumetric term is added to enforce incompressibility.

$$W(I_1, I_4) = c_0 \{ \exp[c_1(I_1 - 3)^2 + c_2(I_4^{1/2} - 1)^4] - 1 \} + c_{\text{PD}}(I_1 - 3) + \kappa \left( \sqrt{I_3} - 1 \right)^2, \quad (25)$$

where  $c_{\text{PD}}$  is a constant chosen to be very small compared to the other effective material moduli and  $\kappa$

Table 1  
Coefficient values for mitral valve tissue

	$c_0$ (kPa)	$c_1$	$c_2$
Anterior	0.399	4.325	1446.5
Posterior	0.414	4.848	305.4

is the compressibility, chosen to be a value much higher than any other effective material moduli. This term is the same as that used in the pressure-displacement formulation (Sussman and Bathe, 1987). In this method, pressure does not need to be separately calculated; the full stress state will be fully calculated by the local plane stress algorithm. The pressure can be calculated from that stress state if desired, but is not required in the numerical method. Thus, the deviatoric and volumetric responses do not have to be isolated from each other. The rest of the modifications (conversion of modified invariants) to the strain-energy function performed in the mixed formulation (Weinberg and Kaazempur-Mofrad, 2005b) are not necessary.

### 3. Numerical tests and results

We have implemented our element in the commercially available finite element software ADINA (Watertown, MA), using  $2 \times 2 \times 2$  Gauss integration for all terms. We first compare the predictions of our model to planar analytical results. Equibiaxial stretch was applied to the element with the material models for anterior and posterior leaflets. The range of deformations here is the same as that in the May-Newman and Yin data (1998), which reflects the range of deformations expected in physiological leaflet function. The numerical results (see Figs. 1 and 2) match the analytical within the limits of numerical accuracy.

To examine the behavior in mixed stress states (membrane and bending stresses), we predict the behavior of a cylindrical arch structure shown in Fig. 3, with large displacements applied. Material properties of the anterior and posterior leaflet are used with constants  $c_{PD} = 1 \times 10^{-5}$  and  $\kappa = 1 \times 10^5$ , and the initial fiber direction is defined running either parallel to the axis of the cylinder or along the circumference of the cylinder. Dimensions are typical of a piece of leaflet

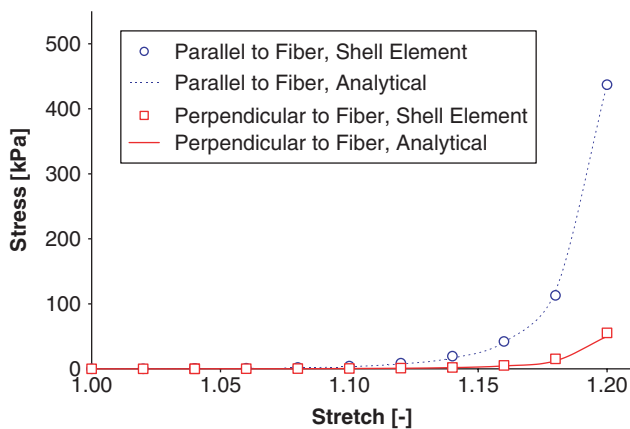


Fig. 1. Numerical and analytical results for equibiaxial stretching of anterior leaflet.

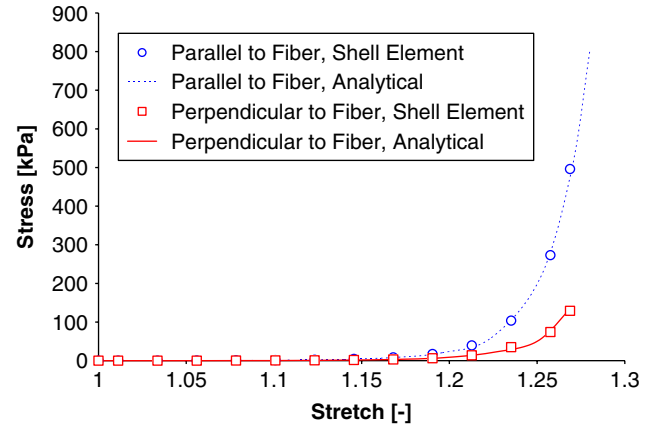


Fig. 2. Numerical and analytical results for equibiaxial stretching of posterior leaflet.

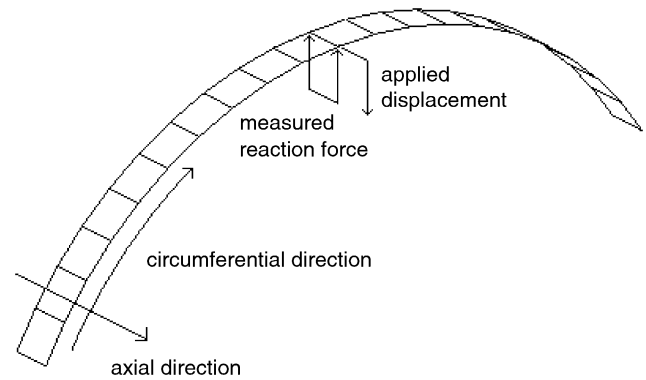


Fig. 3. Geometry of cylindrical test case.

tissue: length of arch of 2.0 cm, height of arch of 0.5 cm, initial thickness of 1.0 mm. In all cases the simulation converged with an applied mid-point displacement up to 0.6 cm. Plots of the reaction force versus the applied displacement are shown in Fig. 4.

### 4. Conclusions

A shell element appropriate for simulating the motion of heart mitral valve leaflets has been presented. This element extends the conventional MITC4 shell element to describe fiber-aligned anisotropy and large deformation. The shell element uses the same DOF as the conventional element, and thus can be readily incorporated into existing finite element software.

The goal is to create a shell element that rigorously predicts the 3D stress state (with the shell stress assumption) of a mitral heart valve leaflet. In this paper, we have used an existing strain-energy function derived and verified in biaxial testing. Simulation of leaflet motion would require a constitutive model

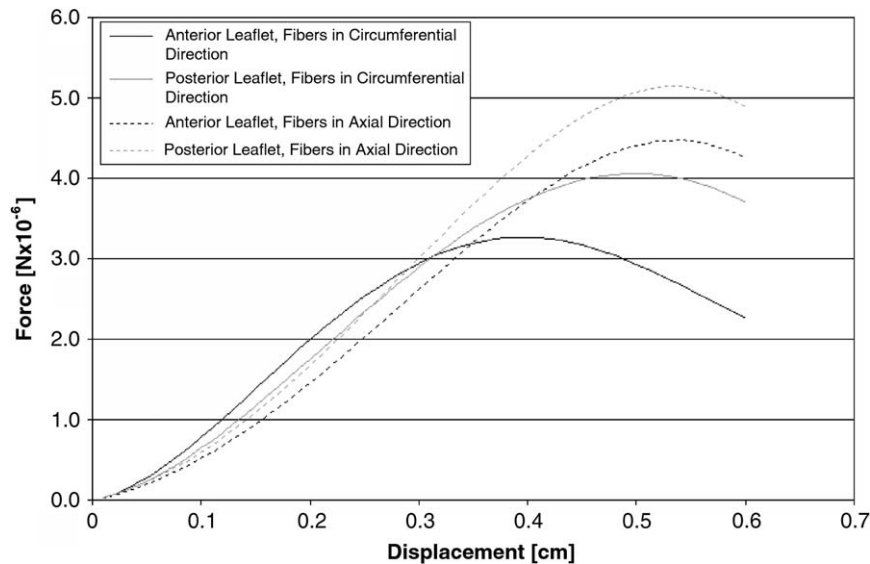


Fig. 4. Force versus displacement plots for cylindrical test case.

verified also in bending and shear. We see the development of this shell element as a step towards determining such a constitutive model.

In this paper, we have extended the MITC4, 5-DOF per node shell element to describe large deformation and transversely isotropic mechanical behavior. This extended element, by using the same DOF as the conventional 4-node shell, can readily be used in finite element codes that already incorporate a 4-node shell, and does not impose the large increase in computation cost associated with adding DOF. This element represents a radical savings in computational expense over our previous method for representing the 3D deformation state, which was using a 27-node mixed-interpolation solid element. Promising future applications of this element include refinements of the leaflet constitutive models, finite element simulations of mitral valve function, and extension to include the layered histology of the leaflet.

## References

- Argyris, J.H., 1982. An excursion into large rotations. *Computer Methods in Applied Mechanics and Engineering* 32, 85–155.
- Basar, Y., Hanskotter, U., et al., 2003. A general high-order finite element formulation for shells at large strains and finite rotations. *International Journal for Numerical Methods in Engineering* 57, 2147–2175.
- Bathe, K.J., 1996. *Finite Element Procedures*. Prentice-Hall, Englewood Cliffs, NJ.
- Betsch, P., Gruttmann, F., et al., 1996. A 4-node finite shell element for the implementation of general hyperelastic 3D-elasticity at finite strains. *Computer Methods in Applied Mechanics and Engineering* 130, 57–79.
- Chapelle, D., Ferent, A., et al., 2004. 3D-shell elements and their underlying mathematical model. *Mathematical Models and Methods in Applied Sciences* 14 (1), 105–142.
- Dvorkin, E.N., 1984. On nonlinear finite element analysis of shell structures. Ph.D. Thesis, Department of Mechanical Engineering, Massachusetts Institute of Technology.
- Dvorkin, E.N., Bathe, K.J., 1984. A continuum mechanics based four-node shell element for general non-linear analysis. *Engineering Computations* 1, 77–88.
- Dvorkin, E.N., Pantuso, D., Repetto, E.A., 1995. A formulation of the MITC4 shell element for finite strain elasto-plastic analysis. *Computer Methods in Applied Mechanics and Engineering* 125, 17–40.
- Einstein, D.R., Kunzelman, K.S., et al., 2004. Haemodynamic determinants of the mitral valve closure sound: a finite element study. *Medical and Biological Engineering and Computing* 42, 832–846.
- Hart, J.D., Peters, G.W.M., et al., 2003. A three-dimensional computational analysis of fluid-structure interaction in the aortic valve. *Journal of Biomechanics* 36, 103–112.
- Klinkel, S., Govindjee, S., 2002. Using finite strain 3D-material models in beam and shell elements. *Engineering Computations* 19 (8), 902–921.
- Kunzelman, K.S., Cochran, R.P., et al., 1993. Finite-element analysis of mitral-valve pathology. *Journal of Long-Term Effects of Medical Implants* 3 (3), 161–170.
- May-Newman, K., Yin, F.C.P., 1998. A constitutive law for mitral valve tissue. *Journal of Biomechanical Engineering* 120, 38–46.
- Simo, J.C., Rifai, M.S., et al., 1990. On a stress resultant geometrically exact shell model. Part IV: variable thickness shells with through-the-thickness stretching. *Computer Methods in Applied Mechanics and Engineering* 81, 91–126.
- Spencer, A.J.M., 1972. *Deformations of Fibre-Reinforced Materials*. Clarendon Press, Oxford.
- Sussman, T., Bathe, K.J., 1987. A finite-element formulation for nonlinear incompressible elastic and inelastic analysis. *Computers and Structures* 26 (1–2), 357–409.

- Sze, K.Y., Zheng, S.J., et al., 2004. A stabilized eighteen-node solid element for hyperelastic analysis of shells. *Finite Elements in Analysis and Design* 40, 319–340.
- Votta, E., Maisano, F., et al., 2002. 3-D computational analysis of the stress distribution on the leaflets after edge-to-edge repair of mitral regurgitation. *Journal of Heart Valve Disease* 11 (6), 810–822.
- Weinberg, E.J., Kaazempur-Mofrad, M., 2005a. On the constitutive models for heart valve leaflet mechanics. *Cardiovascular Engineering* 5 (1), 37–43.
- Weinberg, E.J., Kaazempur-Mofrad, M., 2005b. A large-strain finite element formulation for biological tissues with application to mitral valve mechanics. *Journal of Biomechanics*, in press.